




RESEARCH ARTICLE

10.1029/2020JA028920

Bursty Ion Escape Fluxes at Mars

E. Dubinin¹ , M. Fraenz¹ , M. Pätzold², S. Tellmann², J. Woch¹, J. McFadden³, and L. Zelenyi⁴ 

Key Points:

- Fluxes of oxygen ions escaping the Martian ionosphere with values exceeding their median values by more than a factor of 100 are observed
- Burst fluxes of the high-energy oxygen ions are often related with high values of the simultaneously measured fluxes of the solar wind
- High fluxes of the low-energy oxygen ions are often related with over dense ion clouds observed in the top-side ionosphere of Mars

Correspondence to:

E. Dubinin,
dubinin@mps.mpg.de

Citation:

Dubinin, E., Fraenz, M., Pätzold, M., Tellmann, S., Woch, J., McFadden, J., & Zelenyi, L. (2021). Bursty ion escape fluxes at Mars. *Journal of Geophysical Research: Space Physics*, 126, e2020JA028920. <https://doi.org/10.1029/2020JA028920>

Received 9 NOV 2020
Accepted 24 MAR 2021

¹Max Planck Institute for Solar System Research, Göttingen, Germany, ²Rheinisches Institut fuer Umweltforschung, Abteilung Planetforschung, Cologne, Germany, ³Space Sciences Laboratory, U.C. Berkeley, Berkeley, CA, USA, ⁴Institute of Space Research, Moscow, Russia

Abstract Based on the Mars Atmosphere and Volatile Evolution measurements we have observed cases when the fluxes of oxygen ions escaping the Martian ionosphere exceed their median values by more than a factor of 100. In the Martian tail very high fluxes of the more energetic ($E > 30$ eV) oxygen ions fill the plasma sheet which then becomes much broader than under conditions with median values of ion fluxes. We have analyzed the occurrence of such events in the upper ionosphere near the terminator plane, which is the main source region of ions in the plasma tail. The maximum values of fluxes of oxygen ions with $E > 30$ eV were observed mostly in the hemisphere where the motional electric field imposed by the solar wind is directed outward from the planet. Although high values of the solar wind dynamic pressure and (or) the motional electric field are favorable for the observation of the extreme values of ion fluxes with $E > 30$ eV, there must also be other factors which initiate these events. In particular, we found a close relation of the maximum ion fluxes with the values of the simultaneously measured fluxes of solar wind penetrating into the upper ionosphere. Direct interaction of both plasmas might be a critical factor for the strong growth of the oxygen ion escape. Very high fluxes of the low-energy oxygen ions ($E < 30$ eV) are often related with ion “clouds” with anomalously large number density observed in the upper ionosphere.

1. Introduction

The topside ionosphere is the main ion reservoir supplying the Martian plasma tail. It was shown that this region is very responsive to the variations of the external (solar extreme ultraviolet [EUV] flux, solar wind, and interplanetary magnetic field) and internal (crustal magnetic field) drivers (Dubinin, Fraenz, et al., 2019). As a result, the escaping ion fluxes also reveal strong variations. Lundin, Barabash, Holmström, et al. (2008) estimated the long-term variations in the ion fluxes due to changes in solar wind dynamic pressure to be a factor of 25–30. However, Nilsson et al. (2010) observed that the average ion flux was only 2–3 times higher during periods of large solar wind dynamic pressure. Dubinin et al. (2011) and Dubinin and Fraenz (2015) found a correlation between the solar wind dynamic pressure and ion fluxes in the plasma sheet using biweekly intervals of Mars Express observations. Ion fluxes varied by a factor of ~ 10 in response to solar wind variations. Using the MAVEN data Dubinin, Fraenz, Pätzold, McFadden, Halekas, et al. (2017) observed increase of the flux of oxygen ions in the plasma sheet by a factor of ~ 10 when the solar wind dynamic pressure varied in ~ 25 times.

Effects of solar irradiance on ion fluxes were discussed in (Dong et al., 2017; Dubinin, Fraenz, Pätzold, McFadden, Mahaffy, et al., 2017; Dubinin, Fraenz, Pätzold, Andrews, et al., 2017; Lundin, Barabash, Fedorov, et al., 2008; Lundin et al., 2013; Nilsson et al., 2011; Ramstad et al., 2013, 2015). Ion fluxes observed by Phobos-2 during solar maximum (Lundin et al., 1989; Ramstad et al., 2013) were approximately 10 times higher than fluxes measured by Mars Express during solar minimum (Dubinin et al., 2011; Lundin, Barabash, Holmström, et al., 2008; Nilsson et al., 2011). According to Lundin, Barabash, Fedorov, et al. (2008) a decrease in the EUV flux by a factor of 2.5 leads to a decrease in the outflow of ions with $E \leq 800$ eV also by a factor of 2.5. Analyzing the Mars Atmosphere and Volatile Evolution (MAVEN) data Dong et al. (2017) found that the total escape rate of ions with $E \geq 6$ eV increases by 50% when the EUV irradiance increases by almost the same factor. Using Mars Express data obtained over almost 12 years Dubinin et al. (2017) observed that the trans-terminator fluxes of cold ($E < 50$ eV) oxygen ions increased by a factor of 5–10 when the EUV flux varied in ~ 1.6 times. Ramstad et al. (2015) studied the effect of EUV on ion escape “freezing” the solar wind parameters. The authors did not separate fluxes of low and high-energy ions and found an

© 2021. The Authors.

This is an open access article under the terms of the [Creative Commons Attribution-NonCommercial License](https://creativecommons.org/licenses/by-nc/4.0/), which permits use, distribution and reproduction in any medium, provided the original work is properly cited and is not used for commercial purposes.

increase by a factor of two in the total ion escape between low and high EUV periods for similar conditions in the solar wind.

A large spread of the values in all these studies might be caused by several reasons: by a high temporal variability of ion fluxes; by distinct effects of the solar and solar wind drivers in the different escape channels; by a spatial asymmetry of the ion flow pattern; and by a dependence on ion energy. The authors also discussed variations of the mean or median values of the ion fluxes. Here we analyze a variability of the ion fluxes as a function of different drivers and also focus on their maximum values observed by MAVEN and conditions favorable for their subsistence. It will be shown that the values of oxygen ion fluxes can exceed their median values by more than two orders of magnitude. In past epochs the solar wind was stronger, solar irradiance was higher and ion loss rate should have been much higher than at present. Therefore, it is interesting to study whether these events with very high ion fluxes are related with the Sun and solar wind conditions.

2. Instrumentation

The MAVEN spacecraft arrived at Mars in September 2014 to study the processes in the upper atmosphere/ionosphere and its interaction with solar wind and the consequent escape of atmospheric species to space (Jakosky et al., 2015). MAVEN was inserted into an elliptical orbit with periaapsis and apoapsis of 150 and 6200 km, respectively, and with a period of 4.5 h. In this paper we discuss observations made by the Supra-Thermal And Thermal Ion Composition (STATIC) instrument from December 18, 2014 to May 15, 2018. The STATIC instrument mounted on the actuated payload platform is used to study the escape of planetary ions. It measures energy spectra of ion fluxes in the range of 0.1 eV to 30 keV and the ion composition (McFadden et al., 2015). The measurements allow a retrieval of the velocity distribution functions and their moments (density, velocity, and temperature) for different ion species. We derive the velocity distribution function by joining several STATIC telemetry products (c0, cf, d1, ce, d0, cd, cc, and ca) into a common matrix with a resolution of 32 energy bins, 4 mass bins, 64 spatial bins and 4 s time resolution. For each bin of this matrix the phase space density is calculated. Since the measurements of the low-energy ions in the dense ionosphere and in the planetary wake are affected by the spacecraft (s/c) potential we made corrections using the values of the s/c potential presented by the STATIC team. Calculations of the corrected moments from three-dimensional distribution functions were based on Liouville's theorem (see, e.g., Lavraud & Larson, 2016). Here we focus only on the observations of the flux of the oxygen ions (O^+ and O_2^+ together) which dominate in the topside ionosphere and in the tail. The STATIC observations were complemented by data obtained by the MAVEN EUV instrument (Eparvier et al., 2015) and solar wind monitoring (solar wind ion analyzer, Halekas et al. 2015), and by the measurements of the magnetic field (Connerney et al., 2015). We utilize the interplanetary magnetic field (IMF) orientation on each MAVEN orbit by averaging the MAG data in the upstream solar wind over 30 min. We processed all orbits in order to study the global features without any assumptions about stationarity of the IMF orientation. The full EUV spectrum at Mars is obtained by combining the MAVEN EUV measurements and the observations at Earth orbit on TIMED-SEE and SOLSTICE instruments interpolated to the Mars position at the time when the MAVEN measurements were obtained (EUV L3 data product produced by the EUV team). Monitoring of the solar wind by solar wind ion analyzer is made with high cadence (4 s) measurements of ion velocity distributions in the 30 eV to 25 keV energy range with 14.5% energy resolution and $3.75^\circ \times 4.5^\circ$ angular resolution in the sunward direction. During the orbits when MAVEN was not in the solar wind, we used the measurements in the magnetosheath since the post-shock plasma parameters beyond the terminator plane are rather close to the undisturbed solar wind values. The measurements performed by the Langmuir probe and waves experiment (Andersson et al., 2015) provide us with in-situ measurements of the electron number density (n_e) and temperature (T_e) in the Martian ionosphere.

3. Observations

Figure 1 (left panels) shows the median and maximum values of the total fluxes of oxygen (O^+ and O_2^+) ions measured with time resolution of 16 s by the STATIC instrument during the time period from December 18, 2014 to May 15, 2018. The data are plotted in cylindrical coordinates collecting all observations in

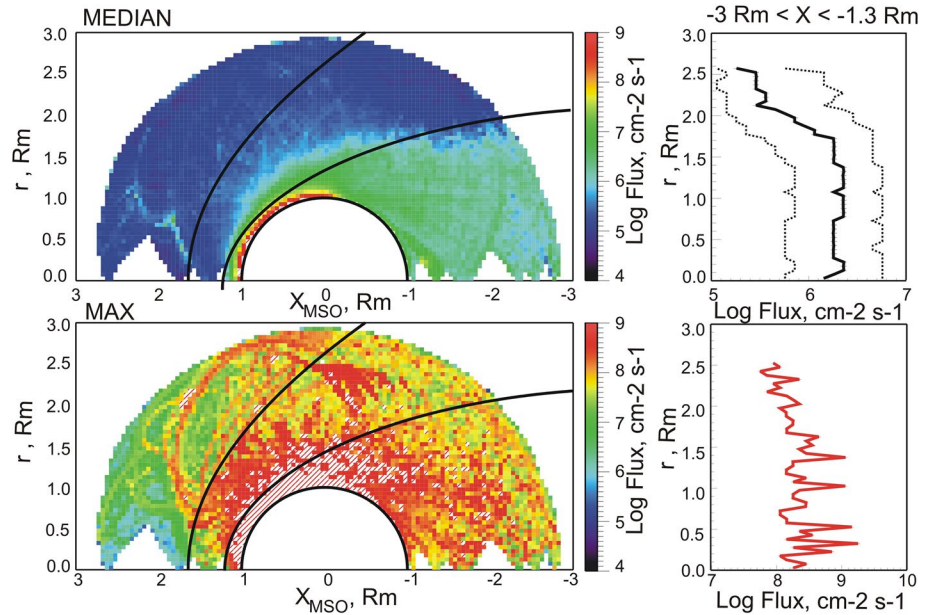


Figure 1. Maps of the median and maximum fluxes of oxygen (O^+ and O_2^+) ions plotted in cylindrical coordinates. In red shaded bins values of fluxes are above $10^9 \text{ cm}^{-2} \text{ s}^{-1}$. Nominal positions of the bow shock and the boundary of the induced magnetosphere are shown. Right panels depict the median (maximum) ion fluxes in the tail ($-3R_m < X_{MSO} < -1.3R_m$) as function of the radial distance r . Dotted curves are the lower and upper quartiles which limit 50% of the data around the median values.

different bins with $0.1 R_M$ size. The median fluxes of oxygen ions are observed mainly within the induced magnetosphere, the nominal boundary of which together with the position of the bow shock are shown by the solid lines (Dubinin et al., 2006). Maximum values of the ion fluxes measured in each bin are significantly higher than the median values and extend to the magnetosheath and solar wind.

Right panels of Figure 1 depict the median (maximum) ion fluxes in the tail ($-3R_m < X_{MSO} < -1.3R_m$) (in the MSO coordinates the X -axis is directed toward the Sun) as function of the radial distance r . Cutoffs at $r \sim 2.5R_m$ appear due to the data coverage. Dotted curves are the lower and upper quartiles which limit 50% of the data around the median values. Already here we observe that maximum values of fluxes are more than a factor 100 higher than the median values. Correspondingly, the ion loss rates through the tail can be estimated as $2.6 \times 10^{24} \text{ s}^{-1}$ (median) and $3.6 \times 10^{26} \text{ s}^{-1}$ (maximum). The calculation of the maximum loss rate assumes that the same conditions apply for the complete cylindrical shell, although the maximum values of ion fluxes measured in each spatial bin might be found under very different conditions and in different time intervals. Nevertheless, it is interesting to examine at what conditions such high fluxes are observed.

Figure 2a shows statistics of the measurements of the different values of the total fluxes of oxygen (O^+ and O_2^+) ions in the tail ($-3R_m < X_{MSO} < -1.3R_m$). The plot also includes some data in the magnetosheath. Black shaded bins indicate only single events. Here we separately present fluxes of low ($E < 30 \text{ eV}$) and high ($E > 30 \text{ eV}$) energy ions. Such a separation is used since the mean (median) fluxes of the low-energy ($\leq 30 \text{ eV}$) and high-energy ($\geq 30 \text{ eV}$) oxygen ions reveal different trends with changes in the solar wind and solar irradiance. The main driver for escape of the high-energy oxygen ions is the solar wind dynamic pressure. On the other hand, the low-energy ion component is not sensitive to solar wind variations and varies with the solar EUV flux (Dubinin, Fraenz, Pätzold, McFadden, Mahaffy, et al., 2017). It is observed from Figure 2a that the events with the maximum values of fluxes in both energy ranges are very rare, that is, $\leq 1\%$ of the total measurements in the Martian tail.

Figures 2b and 2c depict the median values of solar EUV flux and solar wind dynamic pressure during the measurements in each flux bin. We observe that at least for the observations of not very high fluxes of ions with $E > 30 \text{ eV}$, the median values of the EUV flux during the measurements of high fluxes of the

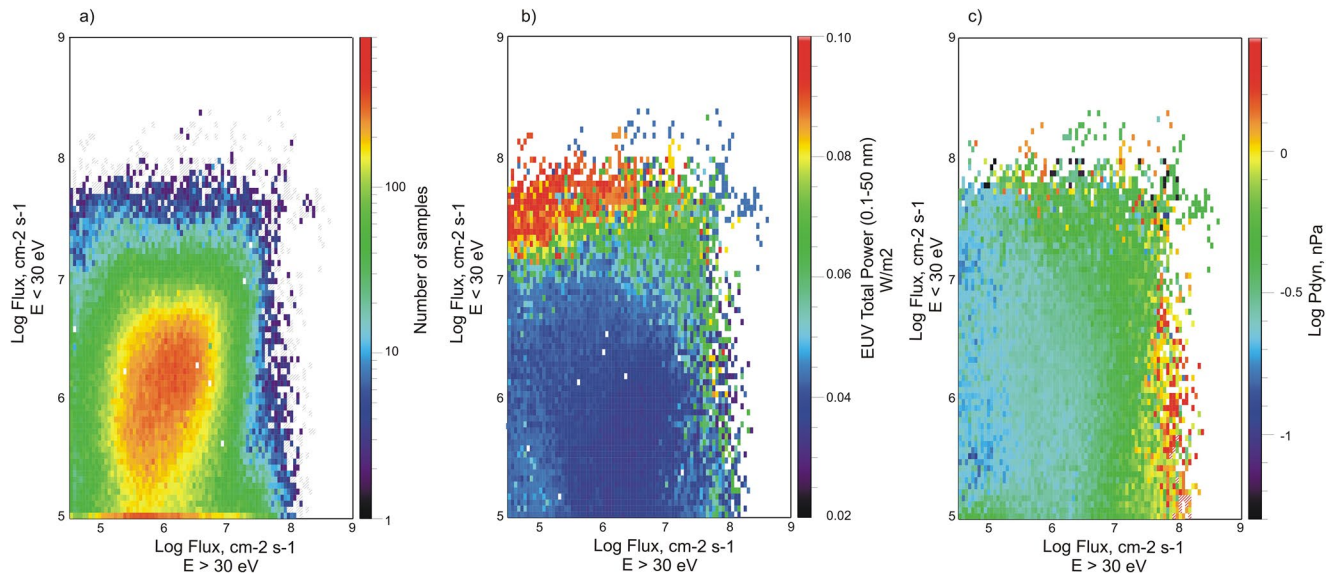


Figure 2. (a) Number of the measurements of the different values of the total fluxes of low-energy ($E < 30$ eV) and high-energy ($E > 30$ eV) oxygen ions in the tail ($-3R_m < X_{MSE} < -1.3R_m$). (b) and (c) Median values of solar EUV flux and solar wind dynamic pressure during the measurements in each flux bin, respectively.

low-energy ($E < 30$ eV) ions correspond to high solar activity (Figure 2b). On the other hand, median values of the solar wind dynamic pressure during the measurements of high ion fluxes with $E > 30$ eV correspond to the strong solar wind, at least during the observations of not very high fluxes of ions with $E < 30$ eV (Figure 2c). This does not mean that the cases with maximum values were recorded only during the time of high solar irradiance or strong solar wind but supports the used ion energy separation, and indicate that these conditions might be favorable for high ion fluxes. On the other hand, we also observe very high fluxes of ions of both energy populations for moderate conditions of the solar wind and the solar EUV flux implying the existence of other drivers.

Figure 3 shows where in the tail median and maximum fluxes of the low-energy and high-energy oxygen ions are observed. It depicts maps of the median values of oxygen ion fluxes in the tail ($-3R_m < X_{MSE} < -1.3R_m$) for the same data set as in Figure 2 plotted in the $B_x - Z_{MSE}$ coordinates, where B_x is the locally observed X -component of the magnetic field and Z_{MSE} is the spacecraft coordinate Z in the Mars solar electric (MSE) coordinate system. In MSE system the X_{MSE} axis coincides with the X_{MSE} axis, while the Y_{MSE} axis is along the cross-flow component of the IMF. Then the Z_{MSE} axis is always along the direction of the motional electric field $E_{sw} = -V_{sw} \times B_{IMF}$. We took the IMF orientation on each MAVEN orbit by averaging the MAG data in the upstream solar wind over 30 min because of frequent fluctuations of the IMF on smaller time intervals. This reference frame is useful since it avoids problems related with multiple crossings of the central current sheet of the tail, that is, around the region where the B_x component changes sign, due to its flapping motions (DiBraccio et al., 2017; Dubinin & Fraenz, 2015; Dubinin, Fraenz, Woch, Zhang, et al., 2012) and reduces uncertainties related to a time lag (\sim several minutes) of the current sheet orientation in response to the IMF variations (Modolo et al., 2012; Romanelli et al. 2018).

Upper (lower) panels show maps of low-energy ($E < 30$ eV) and high-energy ($E > 30$ eV) ions, respectively. It was shown earlier (Dubinin, Fraenz, Pätzold, McFadden, Halekas, et al., 2017) that oxygen ions with different energy occupy different areas in the tail. More energetic ions fill mainly the central part of the tail—plasma sheet, where the $j \times B$ force has its maximum value. The lobes of the tail are filled by oxygen ions with lower energy—from few eV to ~ 10 – 30 eV. These ions are extracted from the Martian ionosphere either by the ambipolar electric field (“polar wind”) or (and) are accelerated by weaker $j \times B$ forces in the draping magnetic field configuration.

Left panels in both rows in Figure 3 depict the median values of the ion fluxes. A spatial separation of low-energy and high-energy ions is clearly seen distinguishing the lobes and the central current sheet. Right

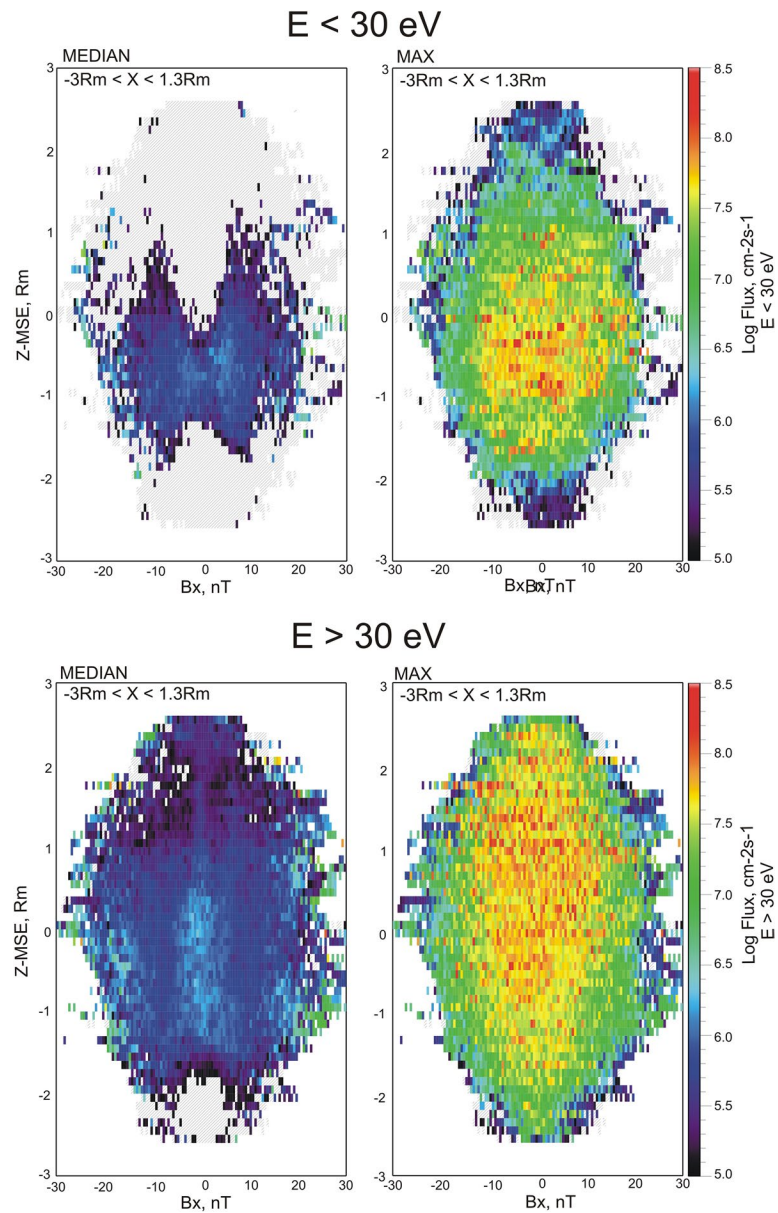


Figure 3. Maps of the median and maximum values of the oxygen ion fluxes in the tail plotted in the $B_x - Z_{MSE}$ variables. Upper (lower) panels show the values of fluxes of oxygen ions with $E < 30$ eV and $E > 30$ eV, respectively. In black shaded bins the fluxes are less than $10^5 \text{ cm}^{-2} \text{ s}^{-1}$.

panels present the maximum values of ions fluxes measured in each bin. Ion fluxes become much higher and the separation between the lobes and the plasma sheet in the central part of the tail almost disappears. Occurrence of the most intense ion fluxes with $E > 30$ eV is higher in the $Z_{MSE} > 0$ hemisphere while the locus of maximum low-energy ion fluxes is shifted to the $Z_{MSE} < 0$ hemisphere, that is, in the agreement with the distribution of mean (median) ion fluxes in the tail (Dubinin, Modolo, et al., 2019).

To identify conditions favorable for the observation of the maximum values of ion fluxes we focus on the measurements in the upper ionosphere of Mars near the terminator plane. It is a transition region through which the plasma in the Martian tail is supplied (Fraenz et al., 2010, 2015). Panels (a) and (b) in Figure 4 show a number of the measurements (samples) in each bin for the measurements of fluxes of oxygen ions with $E < 30$ eV and $E > 30$ eV at solar zenith angles (SZA) in the range $70^\circ - 100^\circ$ and different altitudes (bin size is 25 km), respectively. Black solid curves give the median values. Dotted curves are the quartiles

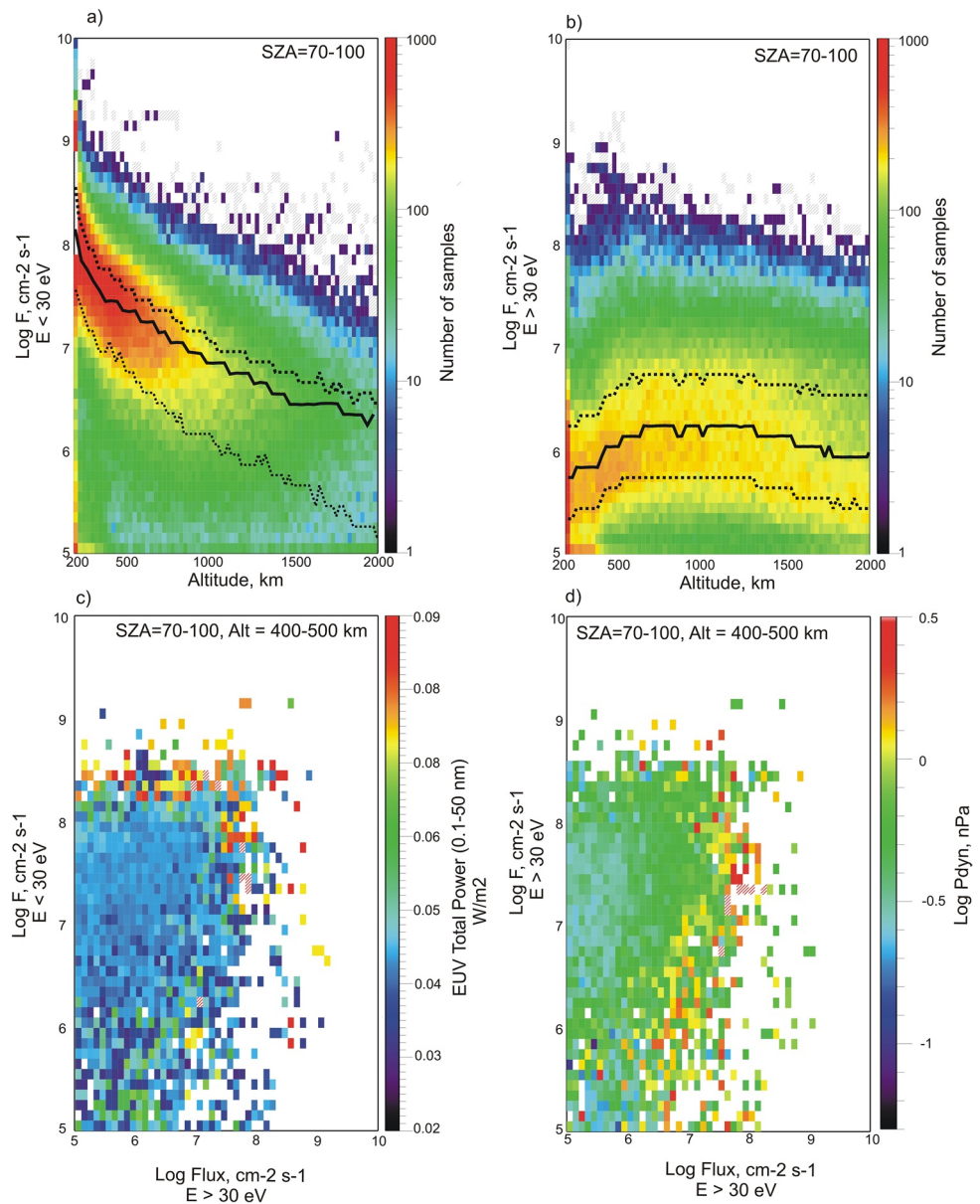


Figure 4. Upper panels show a number of the measurements of fluxes of oxygen ions with $E < 30$ eV (left) and $E > 30$ eV (right) made at different altitudes at solar zenith angles (SZA) $70^\circ - 100^\circ$. Median values and the upper and lower quartiles are shown by the black solid and dotted lines, respectively. Lower panels show the median values of solar EUV flux and solar wind dynamic pressure for the measurements of the low-energy and high-energy oxygen ions at SZA = $70^\circ - 100^\circ$ and Alt = 400–500 km.

which limit 50% of the data around the median values. A strong variability of the flux values is the main feature. Fluxes of low energy ions with median values dominate at almost all altitudes. Fluxes of more energetic ions are more frequently observed at higher altitudes. Their values increase with altitude up to ~ 1000 km and then slightly decrease. There are also cases of the measurements of very high fluxes of low-energy and high-energy ions mostly observed as single events (black shaded bins), but a number of such cases is $\leq 1\%$ as compared to number of samples close to the median values. The values of these maximum fluxes in both energy ranges are comparable.

Figures 4c and 4d show the median values of solar EUV flux and solar wind dynamic pressure in each bin during the measurements of the low-energy and high-energy ions at SZA in the range of $70^\circ - 100^\circ$

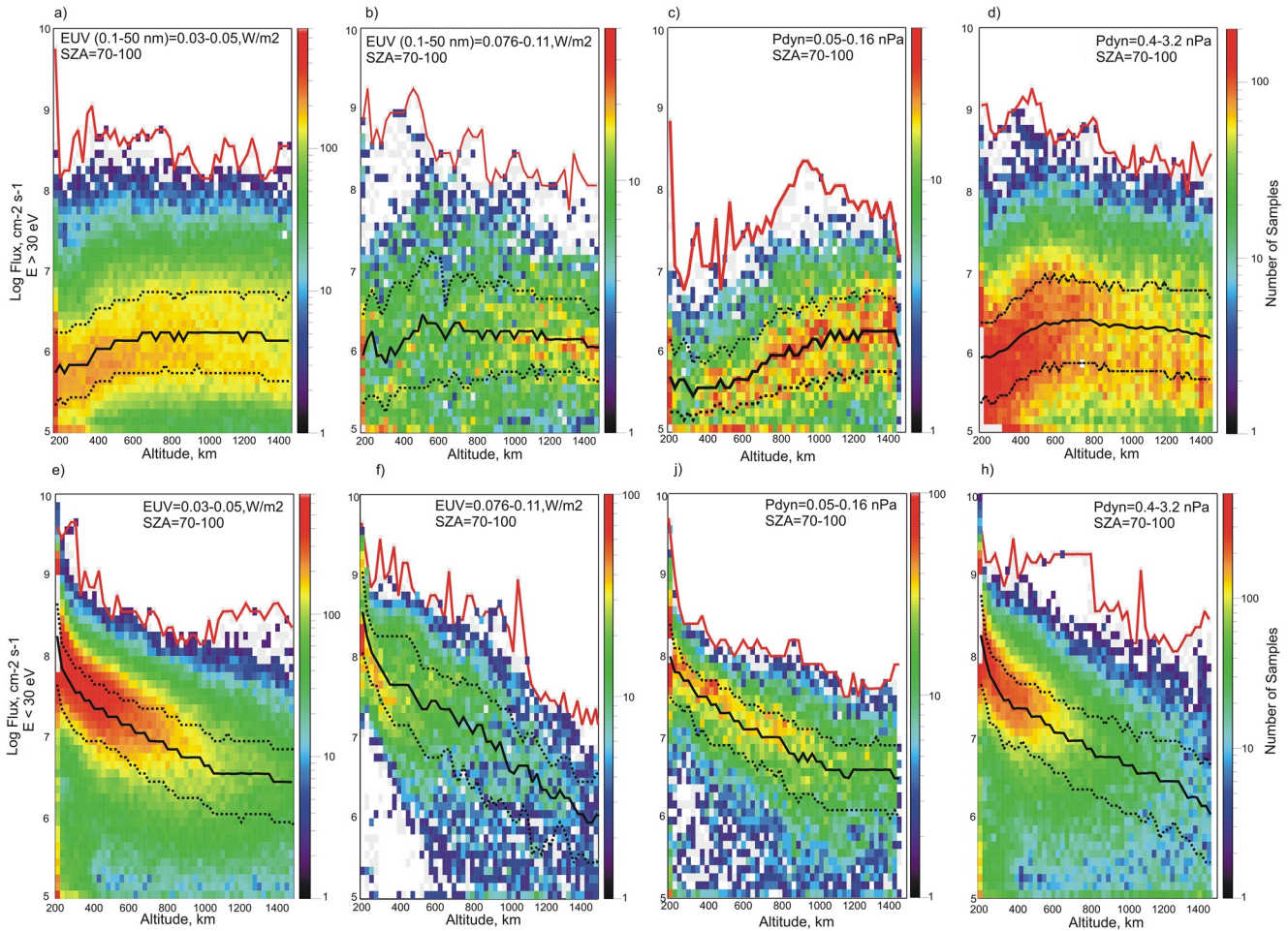


Figure 5. (a) and (b) Statistics of the measurements of fluxes of ions with $E > 30$ eV at $\text{SZA} = 70^\circ - 100^\circ$ and at two different conditions in the solar irradiance. (c) and (d) Statistics of the measurements of fluxes of ions with $E > 30$ eV at two different conditions of the solar wind. Black and red solid curves show the median and maximum values of ion fluxes, respectively. Dotted curves depict the upper and lower quartiles. The lower row (e)–(h) shows similar plots for fluxes of the low-energy ($E < 30$ eV) ions.

and altitudes of 400–500 km, respectively. Similar to Figure 2, we separately present fluxes of low-energy ($E < 30$ eV) and high-energy ($E > 30$ eV) ions. We observe that the median values of the solar irradiance during the measurements of high fluxes of ions with $E < 30$ eV often correspond to high solar activity, while a lot of the measurements of high fluxes of ions with $E > 30$ eV were done during the enhanced solar wind dynamic pressure. On the other hand, we have many cases with very high ion fluxes observed for moderate EUV or solar wind conditions implying that strong solar wind or high solar EUV flux are favorable but often not always necessary for the appearance of very high ion fluxes.

Now we consider in more details a role of different drivers for the very high values of ion fluxes. Figures 5a and 5b present a number of the measurements of fluxes of ions with $E > 30$ eV at $\text{SZA} = 70^\circ - 100^\circ$ and at two different conditions in the solar irradiance. Black and red solid curves show the median and maximum values of ion fluxes, respectively. Dotted curves depict the upper and lower quartiles. We do not observe any significant changes in the values of the median and maximum ion fluxes with the EUV variations ($\text{EUV} = 0.03\text{--}0.05$ W/m² and $\text{EUV} = 0.076\text{--}0.11$ W/m²). Panels (c) and (d) show a number of the measurements of fluxes of ions with $E > 30$ eV with their median and maximum values of fluxes at two different solar wind conditions ($P_{\text{dyn}} = 0.05\text{--}0.16$ nPa) and $P_{\text{dyn}} = 0.4\text{--}3.2$ nPa). At low values of the solar wind dynamic pressure ($P_{\text{dyn}} = 0.05\text{--}0.16$ nPa), the median ion fluxes increase with altitude more smoothly as compared to their values at high P_{dyn} ($P_{\text{dyn}} = 0.4\text{--}3.2$ nPa) although the maximum values of the median fluxes are approximately the same for both regimes in the solar wind. In contrast, the behavior of the maximum ion

fluxes (red curves) with altitude occurs different at low and high P_{dyn} . The absolute values of the maximum ion fluxes are also different implying an important role of P_{dyn} .

The lower row in Figure 5 (panels (e)–(h)) presents similar plots for the measurements of fluxes of ions with $E < 30$ eV. We observe that the median and maximum fluxes of the low energy ions at altitudes below ~ 1000 km significantly increase with increase of the solar EUV flux, but at higher altitudes ion fluxes at weaker EUV radiation become higher. Maximum values of the fluxes of ions with $E < 30$ eV also strongly increase with increase of the solar wind dynamic pressure, while the median values almost not sensitive to variations in P_{dyn} .

Figure 6a shows several examples of the STATIC measurements of fluxes of ions with $E > 30$ eV at $\text{SZA} = 70^\circ\text{--}100^\circ$ which demonstrate some important features. The green curve shows the total fluxes of oxygen ions measured on 20 May 2017 ($P_{dyn} = 0.79$ nPa). Solid and dotted curves depict for comparison the median fluxes and the upper and lower quartiles corresponding to $P_{dyn} = 0.4\text{--}3.2$ nPa. The fluxes measured on 20 May 2017 almost coincide with the maximum values of fluxes observed in all cases at $\text{SZA} = 70^\circ\text{--}100^\circ$. The red curve corresponds to the measurements made during the impact of an interplanetary coronal mass ejection (ICME) in September 2017. The shock related with the ICME arrived on 13 September at 02:52 UT (Lee et al., 2018). During the event MAVEN did not enter the solar wind and therefore there are uncertainties in the solar wind parameters. Results from CME modeling provide proxy peak values of the dynamic pressure in the range 3.4–3.8 nPa. According to Ma et al. (2018) the peak value of the dynamic pressure reached 20.8 nPa at 08:00 UT. During this event we also observe ion fluxes with values close to the maxima. It is important to note that in both cases, the MAVEN measurements were done in the E^+ -hemisphere in which the motional electric field in the solar wind is pointing along the $+Z_{MSE}$ -axis. The dotted red curve in Figure 6a depicts the ion fluxes measured in the opposite E^- -hemisphere on the inbound leg of the same orbit on 13 September (07:20–07:48UT). We observe that ion fluxes in both hemispheres differ by two orders of magnitude implying a very asymmetric ion outflow during this event. Note that in the E^- hemisphere the values of fluxes are within the area limited by the upper and lower quartiles which bound 50% of the data around the median values.

We do not compare here the fluxes measured on both orbital legs on 20 May 2017, since on the inbound part of the orbit the spacecraft sampled the regions with much smaller SZA. But a similar large spatial asymmetry is observed on many other orbits. Figure 6b presents an example of the measurements made on two legs of the orbit on 3 April 2015 in a similar range of the SZA. The solar wind dynamic pressure was rather moderate ($P_{dyn} = 0.6$ nPa). The observations were carried out at EUV (0.1–50 nA) = 0.076 W/m² and therefore we also plot here the median and quartile values for the measurements at EUV = 0.076–0.11 W/m² (solid and dotted black curves). We see that the values of ion fluxes measured at almost the same solar and solar wind conditions show a very large variability controlled only by the position of the spacecraft in the MSE coordinates.

Another important feature of the observations of very high values of the ion fluxes with $E > 30$ eV can be seen in Figures 6c and 6d. Here we show fluxes of oxygen ions (red curves) on the same orbits on 13 September 2017 and 3 April 2015 and fluxes of the solar wind protons (black curves). On 13 September 2017 (the ICME impact), the solar wind plasma penetrates down to ~ 250 km. The region above of ~ 250 km is filled by both plasmas. Spikes of ionospheric plasma are often accompanied by drops in fluxes of the solar wind plasma. Similar features of the direct interaction of the solar wind with the ionospheric plasma are observed on orbit on April 3, 2015, but at less disturbed solar wind conditions. It is worth noting that we cannot distinguish between the solar wind protons and protons of the atmospheric origin picked up by the solar wind flow. Therefore, we also present the fluxes of the low energy ($E \leq 30$ eV) protons (the dotted black curve) and solar wind He^{++} ions multiplied by a factor of 20 (Figure 6c, blue curve). At altitudes above ~ 1000 km fluxes of H^+ and He^{++} ions are well correlated. At smaller distances correlation remains, although the ratio of their fluxes strongly varies. At $h \sim 400$ km and below, the ratio $F(\text{He}^{++})/F(\text{H}^+)$ increases implying a deeper penetration of He^{++} ions, probably, due to their larger Larmor radius. At $h \leq 400$ km the proton fluxes and fluxes of the oxygen ions with $E \geq 30$ eV strongly decrease pointing to a significance of a direct interaction of both plasmas for ion losses. Fluxes of the low-energy protons decrease with altitude at $h \leq 300$ km. At higher altitudes we observe several peaks which correlate with the peaks of the oxygen ions

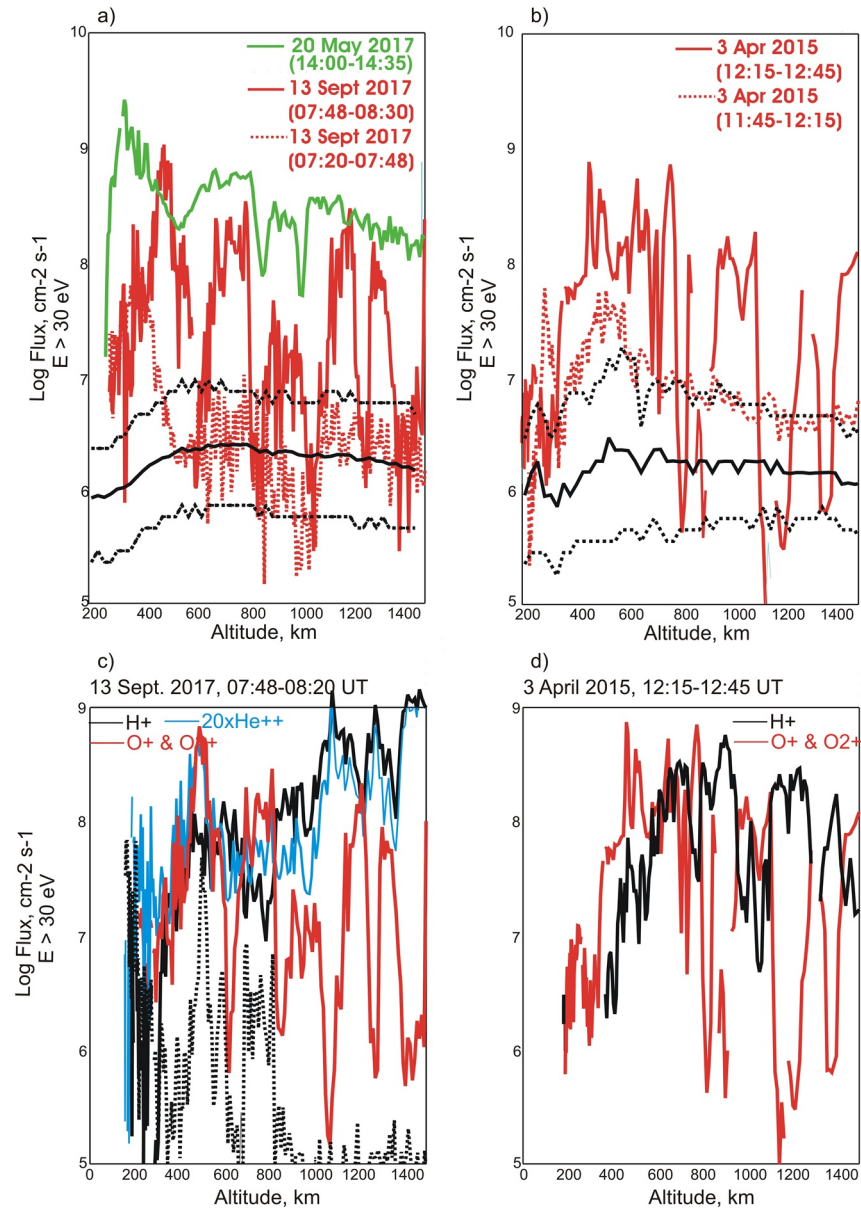


Figure 6. (a) The green curve shows the total fluxes of oxygen ions with $E > 30$ eV measured on 20 May 2017 at $\text{SZA} = 70^\circ\text{--}100^\circ$. Solid and dotted curves are the median fluxes and the upper and lower quartiles corresponding to statistics at $P_{\text{dyn}} = 0.4\text{--}3.2$ nPa. The dotted and solid red curves show the measurements made during the impact of ICME in September 2017 on the inbound and outbound legs, respectively. (b) Similar measurements made on 3 April 2015. Median and quartile values correspond to the measurements at $\text{EUV} = 0.076\text{--}0.11$ W/m². (c) and (d) Fluxes of oxygen ions (red) and solar wind protons (black) as a function of altitude ($\text{SZA} = 70^\circ\text{--}100^\circ$) on the outbound legs of the orbits on September 13, 2017 and on April 3, 2015. The blue curve in Figure 6c depicts fluxes of the He^{++} ions. The dotted black curve shows fluxes of protons with $E \leq 30$ eV.

implying a certain contribution of the atmospheric protons, although their fluxes are significantly lower than fluxes of oxygen ions.

Figure 7 shows the median values of the Z_{MSE} position of MAVEN plotted as a function of both altitude and high-energy ion flux. We see that the maximum fluxes of oxygen ions with $E > 30$ eV are observed mostly in the E^+ -hemisphere.

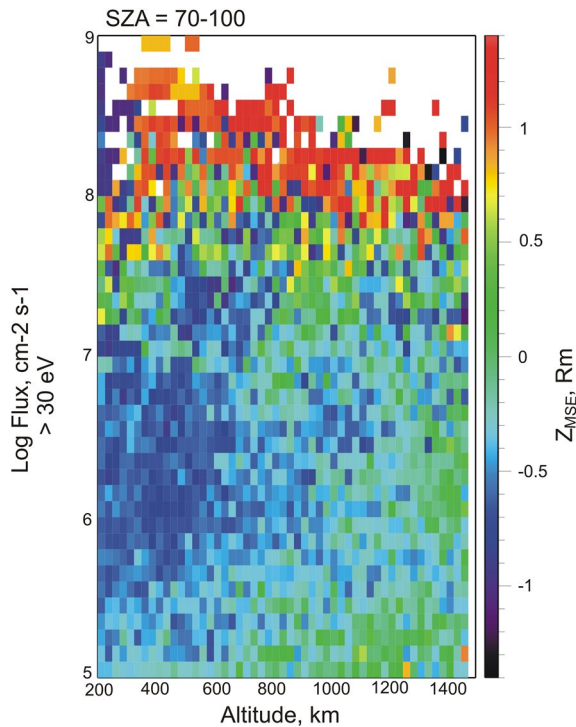


Figure 7. Median values of the Z_{MSE} position of MAVEN plotted as a function of altitude and flux ($E > 30$ eV) for $SZA = 70^\circ$ – 100° .

Figure 8 shows how median (black curves) and maximum (red curves) fluxes of ions with $E > 30$ eV measured at $SZA = 70^\circ$ – 100° and altitude of 400–500 km vary with changes in the solar wind dynamic pressure (a), the motional electric field (b), and the solar EUV flux (c), respectively. Color bars present a number of the measurements in each bin (size of the altitude bin is 25 km). Red squares show the data for orbit on 13 September 2017 (impact by the ICME). As a result of the uncertainty with the solar wind parameters for this case we use two values of the P_{dyn} (7.4 and 20.8). We observe a trend of a sharp increase of the maximum flux values with increase of the solar wind pressure or the motional electric field at $P_{dyn} \leq \sim 1$ nPa and $(V \times B) \leq \sim 0.25$ mV/m, respectively. It is difficult to say whether a decrease of the values at higher P_{dyn} and $(V \times B)$ is related to a pure statistic of the measurements and, for example, the absence of measurements at large Z_{MSE} or has another origin. Large variations in ion fluxes are probably caused by their filamentary structure, as seen, for example, on orbits on September 13, 2017 and April 3, 2015 and by a diversity of fluxes due to a strong axial asymmetry of the escape pattern, in particularly, in the MSE coordinates. In contrast, we do not observe a visible effect of the solar irradiance on values of the maximum ion fluxes.

Figures 9a–9c present similar to Figure 8 plots of effects of different drivers on median and maximum fluxes of low-energy ($E < 30$ eV) oxygen ions at $SZA = 70^\circ$ – 100° and altitudes of 400–500 km. Median values of ion fluxes almost do not vary with changes of the solar wind dynamic pressure and the motional electric field. Maximum values of ion fluxes at first increase with P_{dyn} and $(V \times B)$ and then drop down. Black squares show the fluxes during the ICME impact (13 September 2017). Variations of median fluxes with solar irradiance reveal a substantial increase at

$EUV > 0.08$ W/m² when the EUV flux increases only by a factor of 2, although statistics of the measurements at high EUV is rather poor. The maximum values of ion fluxes show large fluctuations and do not reveal any trend with changes in solar activity.

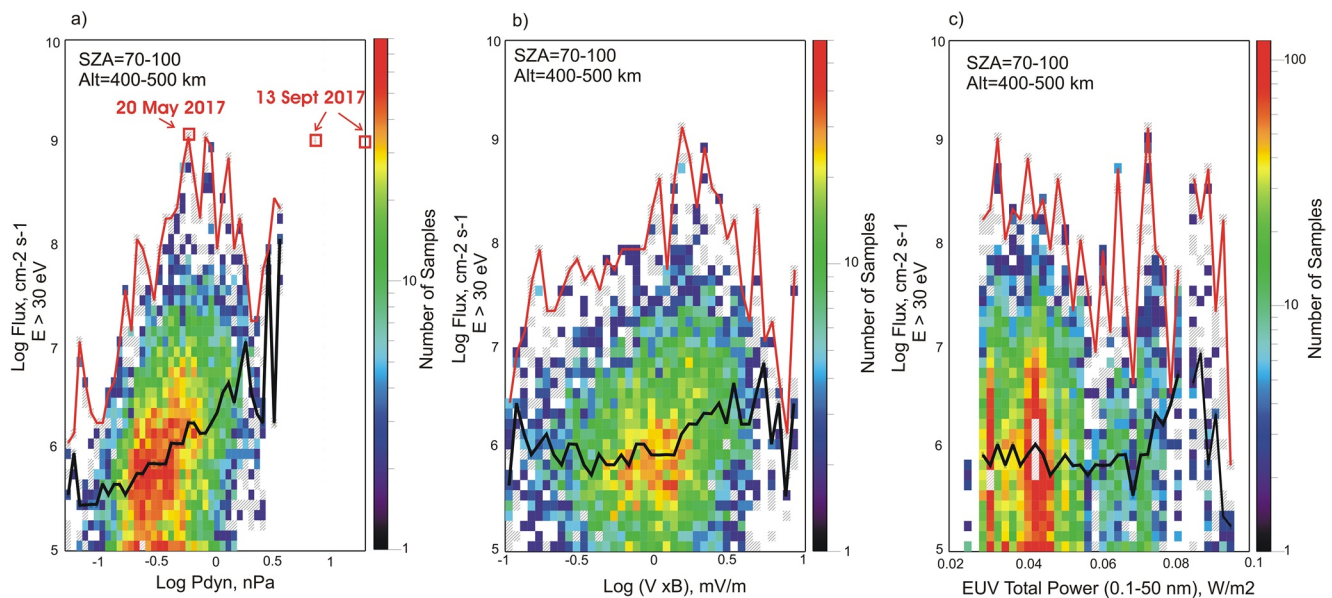


Figure 8. Upper panels: median (black curves) and maximum (red curves) fluxes of ions with $E > 30$ eV measured at $SZA = 70^\circ$ – 100° and altitude of 400–500 km as a function of changes in the solar wind dynamic pressure (a), the motional electric field (b), and the solar EUV flux (c), respectively. Color bars present a number of the measurements in each bin (size of the altitude bin is 25 km). Red squares show the data for orbit on 13 September 2017.

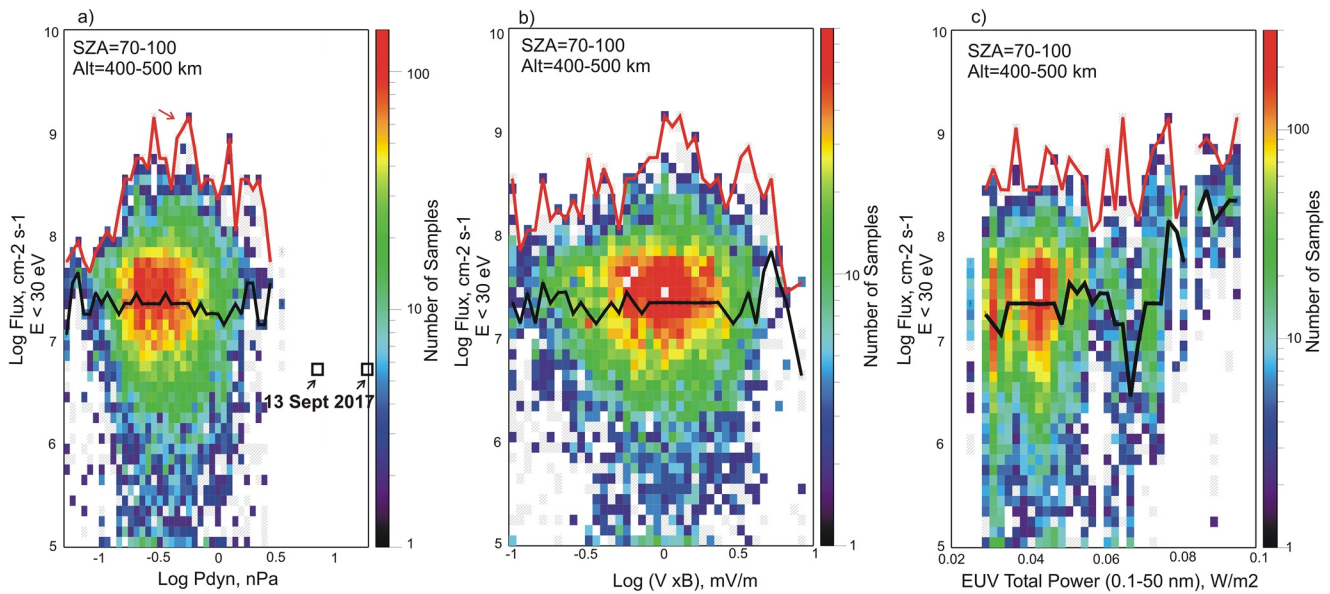


Figure 9. The same as in Figure 8 but for low-energy ion fluxes.

A decrease of the maximum fluxes of low-energy ions at high values of the solar wind pressure and the motional electric field can occur due to the efficient ion acceleration and their conversion to the high-energy population. We can see it, for example, from Figure 10a which depicts the fluxes of the low-energy oxygen ions on the outbound leg of the orbit on 13 September 2017 (blue curve) when an ICME impacted Mars followed by the appearance of very high fluxes of ions with $E > 30$ eV (see Figure 6a). Comparing the ion fluxes with $E > 30$ eV (Figure 6a) and $E < 30$ eV (Figure 10a) we observe a strong decrease of fluxes of the low-energy component, even below the values of the median values. It happens due to conversion of ions

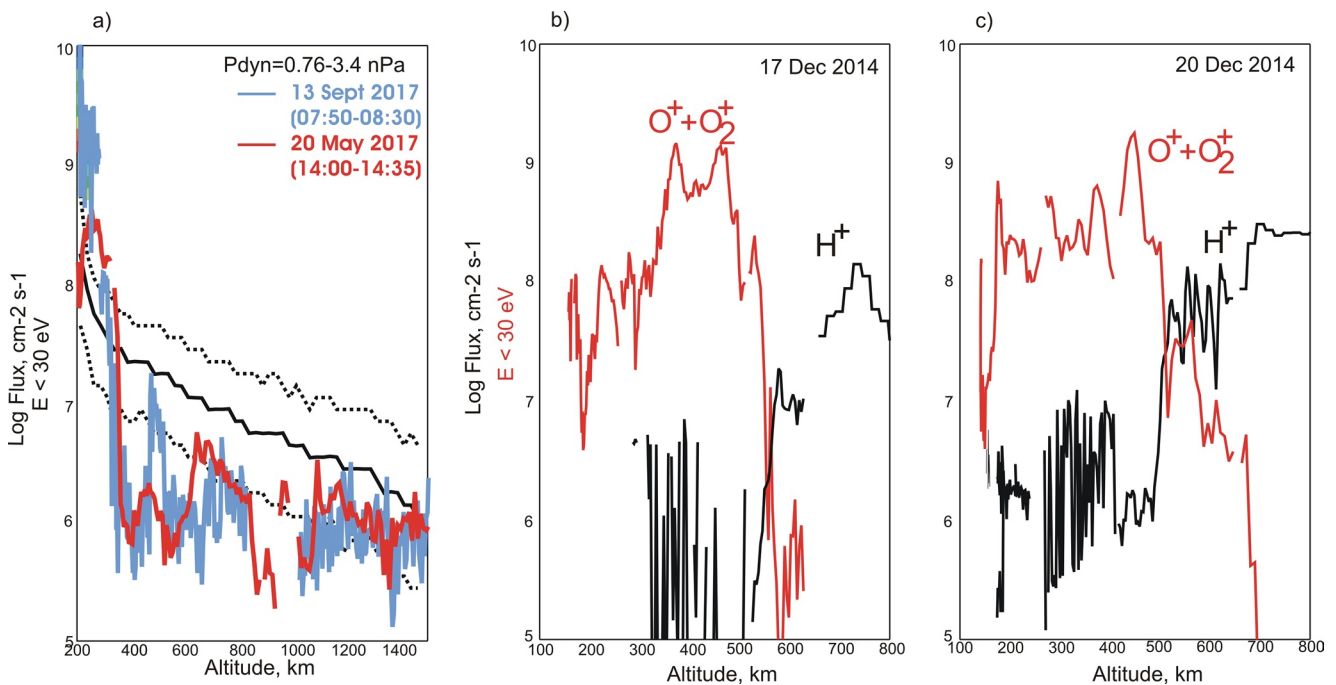


Figure 10. (a) Fluxes of the low-energy oxygen ions on the outbound legs of the orbit on 13 September 2017 (blue curve) and the orbit on 20 May 2017 (red curve). Black curves are the median, upper and lower quartiles corresponding to values of $P_{dyn} = 0.4\text{--}3.2$ nPa. (b) and (c) Examples of the measurements of fluxes of the low-energy oxygen ions (red curves) and solar wind protons (black curves).

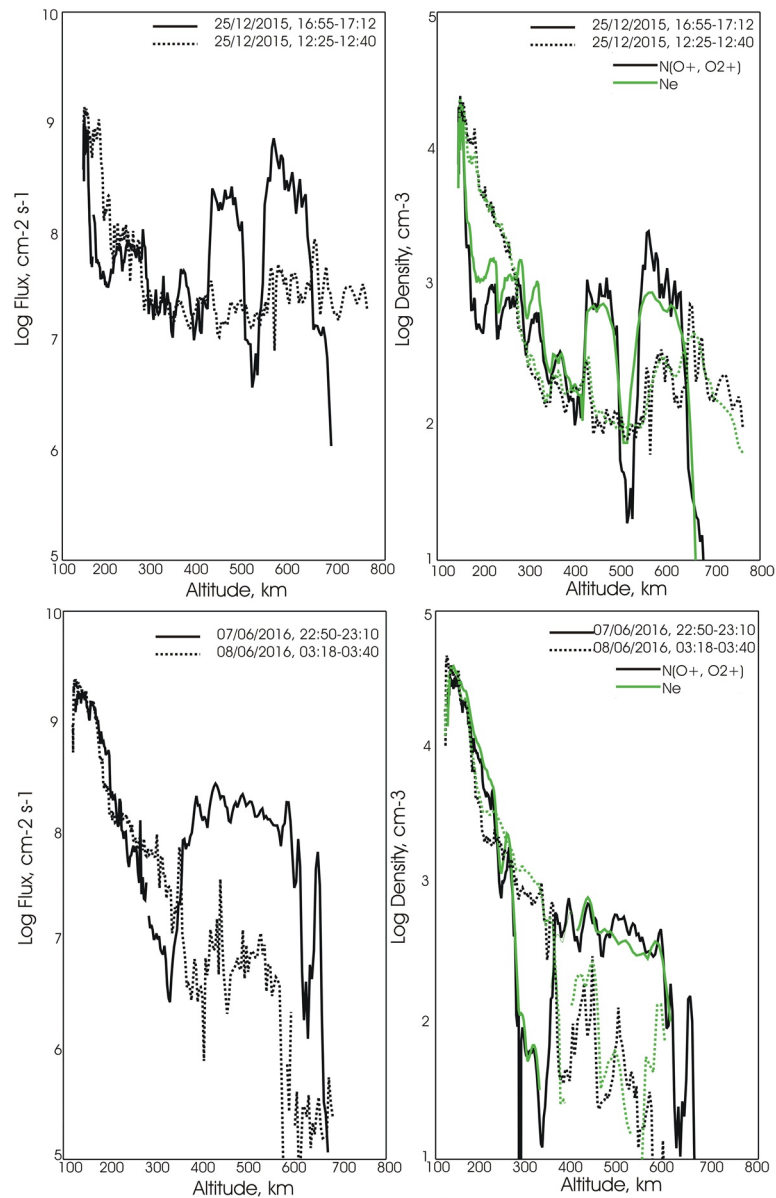


Figure 11. Left panels are examples of the observations of high values of the fluxes of the low energy oxygen ions in the upper ionosphere. Right panels show the ion (black) and electron (green) density profiles. Dotted curves on all panels are the data obtained on the nearby MAVEN orbits.

with low-energy to the high-energy population. As a result, the growth of the total loss rate of oxygen ions during this and similar events might be rather moderate. We observe the same feature on the orbit on 20 May 2017 (red curve) which can be compared with high-energy ion fluxes in Figure 6a. Panels (b) and (c) of Figure 10 demonstrate another important characteristic of the observations of very high fluxes of the low-energy ions. The black (red) curves show fluxes of the solar wind protons (oxygen ions), respectively. The events are observed inside the induced magnetosphere where the direct solar wind contribution is minor. This is valid for all our cases with maximum fluxes of the low-energy ions.

We also found that the cases with very high fluxes of the low-energy oxygen ions are often related with anomalously large number densities in the upper ionosphere. Figure 11 (left panels) show examples of the altitude profiles of low-energy ion fluxes with very high values. We observe structures with large plasma density in the upper ionosphere which resemble similar structures observed at Venus (Brace et al., 1982).

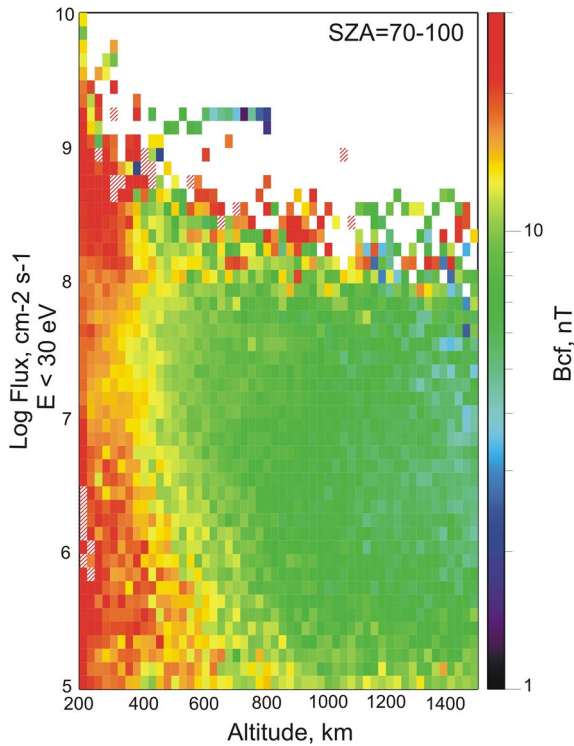


Figure 12. Median values of the cross-flow component B_{cf} measured at SZA = 70°–100° for different values of ion fluxes ($E < 30$ eV). In red shaded bins the magnetic field is larger than 40 nT.

a factor 100. If the fluxes with the maximum values simultaneously fill the cross-section of the tail, the ion loss rate would be about $3.6 \times 10^{26} \text{ s}^{-1}$. We have studied the occurrence of the maximum values of fluxes of ions with $E < 30$ eV and $E > 30$ eV as a function of the solar wind dynamic pressure and the solar EUV flux. We used such a separation in energy based on the observations of different trends in the mean (median) fluxes of the low-energy ($E \leq 30$ eV) and high-energy ($E \geq 30$ eV) ions with changes in the solar wind and solar irradiance (Dubinin, Fraenz, Pätzold, McFadden, Halekas, et al., 2017). Ions with higher energy mainly fill the region adjacent to the current sheet of the magnetic tail (plasma sheet). Their maximum fluxes are also localized in the plasma sheet where the $j \times B$ forces are the strongest. But this region becomes significantly broader. The most intense fluxes are observed in the E^+ -hemisphere. Median fluxes of the low-energy ions fill the tail lobes adjacent to the plasma sheet. For maximum fluxes of these ions the plasma sheet and lobes strongly overlap. Maximum fluxes of low energy ion are more often observed in the E^- -hemisphere. Such a behavior is related to a shift toward the $-Z_{MSE}$ direction of the magnetic tail and the appearance of the ion trail which contains a dense and slowly moving plasma (Dubinin, Modolo, et al., 2019). Median values of the solar wind dynamic pressure and solar EUV flux during the measurements of maximum fluxes of ions with $E > 30$ eV and $E < 30$ eV correspond to disturbed solar wind conditions or high EUV values, respectively. In other words, we observe similar trends for maximum ion fluxes as trends for mean (median) values. On the other hand, we also observe very high ion fluxes for moderate conditions in the solar wind and solar irradiance implying the existence of other drivers. We could not identify a unique driver which might be solely responsible for the appearance of very high ion fluxes in the tail.

We have analyzed the measurements in the upper ionosphere near the terminator plane, from which the oxygen ions supply plasma into the tail. We found a clear relation between the solar wind dynamic pressure or the solar wind motional electric field and the maximum fluxes of ions with $E > 30$ eV, although the positive correlation is only significant up to moderate values of the solar wind parameters. Pure statistics of the measurements for strong solar wind leaves an uncertainty concerning very large values of the solar

In both cases shown in Figure 11 the measurements were done during the moderate solar and solar wind conditions ($P_{dyn} = 0.38$ and 0.63 nPa, EUV(0.1–50 nA) = 0.047 and 0.045 W/m^2 on December 25, 2015 and June 7, 2016, respectively). Right panels show the ion ($O^+ + O_2^+$) (black curves) and the electron (green curves) density profiles measured on the same orbits by two different instruments. Despite of a certain mismatch between the STATIC and Langmuir probe and waves data a clear signature of large-scale structures with very high number densities in the upper ionosphere for cases with high ion fluxes is observed. Dotted curves on the left panels present the measurements with much lower ion fluxes carried out on the nearby MAVEN orbits. We see very different values of the ion fluxes for the same external solar and solar wind conditions implying that the cases with very large low-energy ion fluxes are either local or transient phenomena.

A tailward transport of these large and dense ionospheric structures might be due to an enhanced thermal expansion driven by the ambipolar electric field (Ergun et al., 2016) due to stronger local gradients in the electron density (pressure), or (and) a drag by the magnetic field tensions. Figure 12 shows a plot for the median values of the cross-flow component of the local magnetic field. We see that higher values of the cross-flow field component are favorable for the observations of the maximum ion fluxes.

4. Discussion and Conclusions

In about $\leq 1\%$ of the MAVEN measurements in the Martian tail and near the terminator plane fluxes of oxygen (O^+ and O_2^+) ions escaping Mars are higher than the median values in the corresponding regions by more than

wind dynamic pressure (motional electric field). The maximum values of these ion fluxes are observed in the E^+ hemisphere implying a significant role of the motional electric field in the ion extraction from the ionosphere.

Another important point is that the maximum values of high-energy oxygen ions are often observed with the simultaneously measured fluxes of the solar wind protons. Direct interaction of both plasmas might be a critical factor for the growth of ion sweeping. Alternating structures with strong fluxes of oxygen ions and with penetrating jets of magnetosheath plasma resemble large-amplitude surface waves propagating on the boundary of two plasmas. Such waves can be caused by the Kelvin-Helmholtz (KH) or other magnetohydrodynamic instabilities. Initiation of the KH instability at Mars was suggested by Gurnett et al. (2010) to explain a generation of large-amplitude waves observed in the upper ionosphere. Ruhunusiri et al. (2016) analyzed possible signatures of the KH instability and concluded that non fully developed vortices can appear at the boundary of the induced Martian magnetosphere. Filamentary structures at the boundary of two plasmas were also observed in the simulations made by Terada et al. (2002). The waves in the simulations were generated only in the E^+ -hemisphere that indicates a possible excitation of the modified Rayleigh-Taylor instability for a plasma with unmagnetized ions driven by the ion acceleration in the motional electric field which acts similar to gravity in the classical Rayleigh-Taylor instability ($\mathbf{E} \cdot \nabla n < 0$, Hassam & Huba, 1987). It is interesting to note that such a filamentary structuring is probably a typical phenomenon arising during solar wind interaction with the ionized gaseous shells. They were clearly observed, for example, in the AMPTE artificial comet. G. Haerendel in paper by Szego et al., (2000) explained them as a “clumping instability” generated by a splitting of the piled up magnetic field. Dubinin et al. (1998) suggested that plasma clumps arise due to waves generated by oxygen ion flow through a fluid dominated by the solar wind protons. Plasma filamentation was also observed in the multiple-ion magnetohydrodynamic simulations of the solar wind interaction with weak comets, Mars and Pluto (Bogdanov et al., 1996; Sauer et al., 1996, 1997).

Median values of fluxes of the low-energy ions sharply increase with increase of solar EUV flux. A high solar irradiance is also favorable for initiation of very high ion fluxes but there are also other unknown yet causes responsible for the maximum values. Recently, using the ionosphere sounding radar measurements on Mars Express, Stergiopoulou et al. (2020) have observed isolated cold plasma structures at much higher altitude than normal. The authors also could not find a relation of these structures to a sole driver.

The observations of very high fluxes of ions with $E < 30$ eV are often accompanied by the appearance of large-scale over-dense structures in the upper ionosphere. These structures might be similar to ion “clouds” observed at Venus (Brace et al., 1982). A large variability of ion fluxes in the upper ionosphere observed even on the subsequent orbits implies that such structures probably represent different stages of the ionospheric response to solar wind variations. However, mechanism of their formation is still unknown. We can assume, for example, that continuous variations in the interplanetary magnetic field and magnetic field “penetrated” into the ionosphere and, correspondingly, variations in the forces caused by the magnetic tensions, produce a mismatch between sources and sinks of the ionospheric plasma. As a result, plasma “clouds” can be locally formed under weak dragging conditions and subsequently swapped downstream under a favorable field orientation. Unfortunately, it is difficult to examine such temporal variability in the upper ionosphere using only the in-situ observations by a single spacecraft.

A separation on fluxes of low-energy and high-energy ions used in our analysis is not a strict one. We presented examples when the low-energy component is transformed to the high-energy population due to ion acceleration. It happens, for example, during strong solar wind events. We show here that as a result of such conversion, a total loss rate might be rather moderate even during solar wind events. The observed large cylindrical asymmetry in distribution of very high ion fluxes might also reduce the total ion losses.

Data Availability Statement

MAVEN data are publicly available through the Planetary Data System (<https://pds-ppi.igpp.ucla.edu/mission/MAVEN>).

Acknowledgments

The MAVEN project is supported by NASA through the Mars Exploration Program. Authors ED, MP, ST, wish to acknowledge support from DFG for supporting this work by grants TE 664/4-1 and PA 525/25-1. LZ wish to acknowledge support from the Russian Science Foundation by Grant 20-42-04, 418 and 21-42-04404.

References

Andersson, L., Ergun, R. E., Delory, G. T., Eriksson, A., Westfall, J., Reed, H., et al. (2015). The Langmuir probe and waves (LPW) instrument for MAVEN. *Space Science Reviews*, *195*, 173–198. <https://doi.org/10.1007/s11214-015-0194-3>

Bogdanov, A., Sauer, K., Baumgärtel, K., & Srivastava, K. (1996). Plasma structures at weakly outgassing comets—results from bi-ion fluid analysis. *Planetary and Space Science*, *44*, 519–528. [https://doi.org/10.1016/0032-0633\(95\)00153-0](https://doi.org/10.1016/0032-0633(95)00153-0)

Brace, L. H., Theis, R. F., & Hoegy, W. R. (1982). Plasma clouds above the ionopause of Venus and their implications. *Planetary and Space Science*, *30*, 29–37. [https://doi.org/10.1016/0032-0633\(82\)90069-1](https://doi.org/10.1016/0032-0633(82)90069-1)

Connerney, J. E. P., Espley, J., Lawton, P., Murphy, S., Odom, J., Oliverson, R., & Sheppard, D. (2015). The MAVEN magnetic field investigation. *Space Science Reviews*, *195*(1–4), 257–291. <https://doi.org/10.1007/s11214-015-0169-4>

DiBraccio, G. A., Dann, J., Espley, J. R., Gruesbeck, J. R., Soobiah, Y., Connerney, J. E. P., et al. (2017). MAVEN observations of tail current sheet flapping at Mars. *Journal of Geophysical Research: Space Physics*, *122*, 4308–4324. <https://doi.org/10.1002/2016JA023488>

Dong, Y., Fang, X., Brain, D. A., McFadden, J. P., Halekas, J. S., Connerney, J. E. P., et al. (2017). Seasonal variability of Martian ion escape through the plume and tail from MAVEN observations. *Journal of Geophysical Research: Space Physics*, *122*, 4009. <https://doi.org/10.1002/2016JA023517>

Dubinin, E., & Fraenz, M. (2015). Magnetotails of Mars and Venus. In A. Keiling, C. M. Jackman, & P. A. Delamere (Eds.), *Magnetotails in the solar system*. John Wiley & Sons, Inc. <https://doi.org/10.1002/9781118842324.ch3>

Dubinin, E., Fraenz, M., Fedorov, A., Lundin, R., Edberg, N., Duru, F., & Vaisberg, O. (2011). Ion energization and escape on Mars and Venus. *Space Science Reviews*, *162*, 173–211. <https://doi.org/10.1007/s11214-011-9831-7>. <https://doi.org/10.1007/978-1-4614-3290-6-6>

Dubinin, E., Fraenz, M., Pätzold, M., Andrews, D., Vaisberg, O., Zelenyi, L., & Barabash, S. (2017b). Martian ionosphere observed by Mars Express. 2. Influence of solar irradiance on upper ionosphere and escape fluxes. *Planetary and Space Science*, *144*, 132.

Dubinin, E., Fraenz, M., Pätzold, M., McFadden, J., Halekas, J. S., DiBraccio, G. A., et al. (2017c). The effect of solar wind variations on the escape of oxygen ions from Mars through different channels: MAVEN observations. *Journal of Geophysical Research: Space Physics*, *122*, 11,285–311,301. <https://doi.org/10.1002/2017JA024741>

Dubinin, E., Fraenz, M., Pätzold, M., McFadden, J., Mahaffy, P. R., Eparvier, F., et al. (2017). Effects of solar irradiance on the upper ionosphere and oxygen ion escape at Mars: MAVEN observations. *Journal of Geophysical Research: Space Physics*, *122*, 7142. <https://doi.org/10.1002/2017JA024126>

Dubinin, E., Fraenz, M., Pätzold, M., Woch, J., McFadden, J., Halekas, J. S., et al. (2019a). Expansion and shrinking of the Martian topside ionosphere. *Journal of Geophysical Research: Space Physics*, *124*. <https://doi.org/10.1029/2019JA027077>

Dubinin, E., Fraenz, M., Woch, J., Zhang, T. L., Wei, J., Fedorov, A., et al. (2012). Bursty escape fluxes in plasma sheets of Mars and Venus. *Geophysical Research Letters*, *39*(1), a. <https://doi.org/10.1029/2011GL049883>

Dubinin, E., Fränz, M., Woch, J., Roussos, E., Barabash, S., Lundin, R., et al. (2006). Plasma morphology at Mars. Aspera-3 observations. *Space Science Reviews*, *126*, 209–238. <https://doi.org/10.1007/s11214-006-9039-4>

Dubinin, E., Modolo, R., Fraenz, M., Pätzold, M., Woch, J., Chai, L., et al. (2019b). The induced magnetosphere of Mars: Asymmetrical topology of the magnetic field lines. *Geophysical Research Letters*, *46*. <https://doi.org/10.1029/2019GL084387>

Dubinin, E., Sauer, K., Baumgärtel, K., & Srivastava, K. (1998). Multiple shocks near Mars. *Earth Planet and Space*, *50*, 279–287. <https://doi.org/10.1186/bf03352114>

Eparvier, F. G., Chamberlin, P. C., Woods, T. N., & Thiemann, E. M. B. (2015). The solar extreme ultraviolet monitor for MAVEN. *Space Science Reviews*, *195*, 293–301. <https://doi.org/10.1007/s11214-015-0195-2>

Ergun, R. E., Andersson, L. A., Fowler, C. M., Woodson, A. K., Weber, T. D., Delory, G. T., et al. (2016). Enhanced O₂⁺ loss at Mars due to an ambipolar electric field from electron heating. *Journal of Geophysical Research: Space Physics*, *121*, 4668. <https://doi.org/10.1002/2016JA022349>

Fraenz, M., Dubinin, E., Andrews, D., Barabash, S., Nilsson, H., & Fedorov, A. (2015). Cold ion escape from the Martian ionosphere. *Planetary and Space Science*, *119*(15), 92–102. <http://dx.doi.org/10.1016/j.pss.2015.07.012>

Fraenz, M., Dubinin, E., Nielden, E., Woch, J., Barabash, S., Lundin, R., & Fedorov, A. (2010). Transterminator ion flow in the Martian ionosphere. *Planetary and Space Science*, *58*, 1442–1454. <http://dx.doi.org/10.1016/j.pss.2010.06.009>

Gurnett, D. A., Morgan, D. D., Duru, F., Akalin, F., Winningham, J. D., Frahm, R. A., et al. (2010). Large density fluctuations in the Martian ionosphere as observed by the Mars Express radar sounder. *Icarus*, *206*, 83–94. <https://doi.org/10.1016/j.icarus.2009.02.019>

Halekas, J. S., Taylor, E. R., Dalton, G., Johnson, G., Curtis, D. W., McFadden, J. P., et al. (2015). The solar wind ion analyzer for MAVEN. *Space Science Reviews*, *195*, 125–151. <https://doi.org/10.1007/s11214-013-0029-z>

Hassam, A. B., & Huba, J. D. (1987). Structuring of the Ampte magnetotail barium releases. *Geophysical Research Letters*, *14*, 60–63. <https://doi.org/10.1029/gl014i001p00060>

Jakosky, B. M., Lin, R. P., Grebowsky, J. M., Luhmann, J. G., Mitchell, D. F., Beutelschies, G., et al. (2015). The Mars Atmosphere and Volatile Evolution (MAVEN) mission. *Space Science Reviews*, *195*(1–4), 3–48. <https://doi.org/10.1007/s11214-015-0139-x>

Lavraud, B., & Larson, D. E. (2016). Correcting moments of in situ particle distribution functions for spacecraft electrostatic charging. *Journal of Geophysical Research: Space Physics*, *121*, 8462–8474. <https://doi.org/10.1002/2016JA022591>

Lee, C. O., Jakosky, B. M., Luhmann, J. G., Brain, D. A., Mays, M. L., Hassler, D. M., et al. (2018). Observations and impacts of the 10 September 2017 solar events at Mars: An overview and synthesis of the initial results. *Geophysical Research Letters*, *45*, 8871–8885. <https://doi.org/10.1029/2018gl079162>

Lundin, R., Barabash, S., Fedorov, A., Holmström, M., Nilsson, H., Sauvaud, J.-A., & Yamauchi, M. (2008). Solar forcing and planetary ion escape from Mars. *Geophysical Research Letters* *35*, L09203. <https://doi.org/10.1029/2007GL032884>

Lundin, R., Barabash, S., Holmström, M., Nilsson, H., Futaana, Y., Ramstad, R., et al. (2013). Solar cycle effects on the ion escape from Mars. *Geophysical Research Letters*, *40*, 6028–6032. <https://doi.org/10.1002/2013GL058154>

Lundin, R., Barabash, S., Holmström, M., Nilsson, H., Yamauchi, M., Fraenz, M., & Dubinin, E. M. (2008). A comet-like escape of ionospheric plasma from Mars. *Geophysical Research Letters* *35*, L18203. <https://doi.org/10.1029/2008GL034811>

Lundin, R., Zakharov, A., Pellinen, R., Borg, H., Hultqvist, B., Pissarenko, N., et al. (1989). First measurements of the ionospheric plasma escape from Mars. *Nature*, *341*, 609–612. <https://doi.org/10.1038/341609a0>

Ma, Y., Fang, X., Halekas, J. S., Xu, S., Russell, C. T., Luhmann, J. G., et al. (2018). The impact and solar wind proxy of the 2017 September ICME event at Mars. *Geophysical Research Letters*, *45*, 7248–7256. <https://doi.org/10.1029/2018gl077707>. <https://doi.org/10.1029/2018GL077707>

McFadden, J. P., Kortmann, O., Curtis, D., Dalton, G., Johnson, G., Abiad, R., et al. (2015). MAVEN SupraThermal and Thermal Ion Composition (STATIC) instrument. *Space Science Reviews*, *195*, 199–256. <https://doi.org/10.1007/s11214-015-0175-6>

- Modolo, R., Chanteur, G. M., & Dubinin, E. (2012). Dynamic Martian magnetosphere: Transient twist induced by a rotation of the IMF. *Geophysical Research Letters*, 39, a. L01106. <https://doi.org/10.1029/2011GL049895>
- Nilsson, H., Carlsson, E., Brain, D. A., Yamauchi, M., Holmström, M., Barabash, S., et al. (2010). Ion escape from Mars as a function of solar wind conditions: A statistical study. *Icarus*, 206, 40–49. <https://doi.org/10.1016/j.icarus.2009.03.006>
- Nilsson, H., Edberg, N. J. T., Stenberg, G., Barabash, S., Holmström, M., Futaana, Y., et al. (2011). Heavy ion escape from Mars, influence from solar wind conditions and crustal magnetic fields. *Icarus*, 215, 475–484. <https://doi.org/10.1016/j.icarus.2011.08.003>
- Ramstad, R., Barabash, S., Futaana, Y., Nilsson, H., Wang, X.-D., & Holmström, M. (2015). The Martian atmospheric ion escape rate dependence on solar wind and solar EUV conditions: I. Seven years of Mars Express observations. *Journal of Geophysical Research: Planets*, 120, 1298–1309. <https://doi.org/10.1002/2015JE004816>
- Ramstad, R., Futaana, Y., Barabash, S., Nilsson, H., Martin del Campo B, S., Lundin, R., & Schwingenschuh, K. (2013). Phobos 2/ASPERA data revisited: Planetary ion escape rate from Mars near the 1989 solar maximum. *Geophysical Research Letters*, 40, 477–481. <https://doi.org/10.1002/grl.50149>
- Romanelli, N., Modolo, R., Leblanc, F., Chaufray, J.-Y., Hess, S., Brain, D., et al. (2018). Effects of the crustal magnetic fields and changes in the IMF orientation on the magnetosphere of Mars: MAVEN observations and LatHyS results. *Journal of Geophysical Research: Space Physics*, 123(7), 5315–5333. <https://doi.org/10.1029/2017JA025155>
- Ruhunusiri, S., Halekas, J. S., McFadden, J. P., Connerney, J. E. P., Espley, J. R., Harada, Y., et al. (2016). MAVEN observations of partially developed Kelvin-Helmholtz vortices at Mars. *Geophysical Research Letters*, 43, 4763–4773. <https://doi.org/10.1002/2016GL068926>
- Sauer, K., Bogdanov, A., Baumgärtel, K., & Dubinin, E. (1996). Bi-ion discontinuities at weak solar wind massloading. *Physica Scripta*, T63, 111–118. <https://doi.org/10.1088/0031-8949/1996/t63/017>
- Sauer, K., Lipatov, A., Baumgärtel, K., & Dubinin, E. (1997). Solar wind-Pluto interaction revised. *Advances in Space Research*, 20(2), 295–299. [https://doi.org/10.1016/s0273-1177\(97\)00551-6](https://doi.org/10.1016/s0273-1177(97)00551-6)
- Stergiopoulou, K., Andrews, D. J., Edberg, N. J. T., Halekas, J., Kopf, A., Lester, M., et al. (2020). Mars Express observations of cold plasma structures in the Martian magnetotail. *Journal Of Geophysical Research: Space Physics*, 125, 10. <https://doi.org/10.1029/2020JA028056>
- Szegő, K., Glassmeier, K.-H., Bingham, R., Bogdanov, A., Fisher, C., Haerendel, G. (2000). Physics of mass-loaded plasmas. *Space Science Reviews*, 94, 429–671. <https://doi.org/10.1023/a:1026568530975>
- Terada, N., Machida, S., & Shinagawa, H. (2002). Global hybrid simulation of the Kelvin-Helmholtz instability at the Venus ionopause. *Journal of Geophysical Research*, 107(A12), 30. <https://doi.org/10.1029/2001JA009224>